Highly nonlinear solitary waves in chains of ellipsoidal particles

Duc Ngo, Devvrath Khatri, and Chiara Daraio

Phys. Rev. E **84**, 026610 — Published 16 August 2011

DOI: 10.1103/PhysRevE.84.026610

Highly nonlinear solitary waves in chains of ellipsoidal particles

Duc Ngo[1], Devvrath Khatri[1], and Chiara Daraio[1,2]

Graduate Aerospace Laboratories (GALCIT)[1] and Applied Physics[2], California Institute of Technology, Pasadena, CA 91125, USA.

Abstract

We study the dynamic response of a one-dimensional chain of ellipsoidal particles excited by a single compressive impulse. We detail the Hertzian contact theory describing the interaction between two ellipsoidal particles under compression, and use it to model the dynamic response of the system. We observe the formation of highly nonlinear solitary wave in the chain, and we also study their propagation properties. We measure experimentally the traveling pulse amplitude (force), the solitary wave speed and the solitary wave width. We compare these results with theoretical predictions in the long wavelength approximation, and with numerical results obtained with a discrete particle model and with finite element simulations. We also study the propagation of highly nonlinear solitary waves in the chain with particles arranged in different configurations to show the effects of the particle's geometry on the wave propagation characteristics and dissipation. We find very good agreement between experiment, theory and simulations for all the ranges of impact velocity and particles' arrangement investigated.

I. Introduction

One-dimensional chains consisting of spherical particles have been extensively studied in the literature and are known to present highly nonlinear dynamic properties [1-19]. When the chains are uncompressed, they support the formation and propagation of compact solitary waves that have been predicted theoretically [1], observed numerically [1,6] and experimentally [4,5]. These systems derive their unique characteristics from a double nonlinearity in the particles interaction: a power-law type contact potential in compression and a zero tensile strength. One of the fundamental characteristics of such systems is their high degree of tunability in terms of control over the traveling pulses width, speed and the number of separated pulses that can be generated in the chain [2,3,9,13-16]. The tunability of these systems is evident when the addition of static precompression on the chain of particles enables the system to change from the highly nonlinear, to the weakly nonlinear, to the linear wave dynamics regime [2,3,5,13]. Changing the type and duration of the initial excitation applied to the system, it is possible to generate single or train of pulses with respective amplitudes [2,14]. Changing the particle diameters, the particle material properties and/or their periodicity, it is also possible to change the solitary waves' amplitude and traveling speed [9,13,15,16]. This ability to control the wave properties in such chains has been proposed for a variety of practical engineering applications, for example it could be employed for shock absorbing materials [7,12,19,21], vibration damping [20], sound scramblers [9,10] and sound focusing [22].

In this paper we explore the effects of the particle geometry and orientation on the formation and propagation of highly nonlinear solitary wave. The role of particle geometry on the dynamic response of granular materials was studied earlier using elliptical disks of hysteretic photoelastic polymers [23]. Here, we experimentally test chains composed of linear elastic, uniform bodies of

revolutions (ellipsoids)and compare the results with theoretical predictions based on the long wavelength approximation for highly nonlinear wave propagation. We employ two different numerical approaches to model the response of the chain, the first method is one-dimensional discrete particles' dynamics (DP) and the second method is a fully three-dimensional finite element (FE) model. The numerical results show good agreement with each other, with the theoretical predictions and experimental observations.

The paper is organized as follows: In Section II we describe the experimental set up, in Section III we briefly present the Herztian contact interaction law for ellipsoidal particles. Section IV presents the long wavelength theory for highly nonlinear wave propagation adapted to a uniform chain of ellipsoidal particles. Section V and VI describe the DP and FE numerical models. In Section VII we present a detail discussion and comparison of the results obtained. We end the paper with conclusions and considerations on their future applicability.

II. Experimental Set-up

We assembled chains of 20 and 50 stainless steel (type 316) ellipsoidal particles (Fig. 1(a,b), supplied by Kramer Industries) stacked along their minor axis direction in a vertical aluminum guide (Fig. 1(c)). Each particle had a mass m=0.925±0.001 g; the minor axis was D=4.72±0.01 mm long and the major axis was L=10.16±0.01 mm long. The modulus of elasticity (E) was equal to 193 GPa and the Poisson's ratio (v) was equal to 0.3 [24]. Two of the ellipsoidal particles in the chain were instrumented as sensors, and placed in the chain at selected locations. The instrumented particles were custom fabricated in our laboratory by introducing a piezoelectric (lead zirconate titanate) sheet (3 mm side plate with thickness 0.5 mm) with custom micro-miniature wiring (supplied by Piezo Systems Inc.) between two portions of an ellipsoidal

particle (Fig. 1(d)). The particles were cut along their major diameter direction and carved to accommodate wires. The final assembly of the sensor particles was achieved following a procedure similar to the one described in [15,16] for spherical particles. All the sensors were pre-calibrated to obtain the relation between voltage output from the oscilloscope and the corresponding force on the particle assuming conservation of linear momentum. Experimental data from the sensors were collected using a Tektronix oscilloscope (TDS 2014). To excite the traveling waves in the system, the chain was subsequently impacted with strikers of different masses (0.45 g, 0.98 g, and 3.79 g).The striker's impact velocity was varied by releasing the striker from different heights, ranging from 7 mm to 48.6 mm. We recorded force-time signals detected by sensors placed at particle number 7 and 12 from the top of the chain to study the properties of the propagating waves. We calculated their average wave speed (V_s) as $V_s = d/TOF$, where d is the distance between the centers of sensor particles, and TOF is the time of flight, which is the time taken by the wave peak (maximum force) to travel between the two instrumented particles. The average maximum force ($F_{m,e}$) of the propagating pulses was determined by taking the average of the force amplitudes detected at sensor particles (i.e. particle number 7 and 12).

III. Contact Interaction Between Ellipsoidal Particles

The interaction between two ellipsoidal particles under an applied compressive load is characterized by an elliptical contact area which is different from the circular contact area observed in the interaction between two spherical particles. A general contact law accounting for the elliptical contact area based on Hertz assumptions was presented in [25] and is briefly summarized here. We consider two ellipsoidal particles initially in contact with each other at point O as shown in Fig. 1(b). In this model, the contact properties are taken to satisfy all the

Hertzian contact theory's assumptions: (i) The contact surfaces are non-conforming, continuous and frictionless; (ii) The strains are small and the material response is purely elastic; (iii) The contact area is very small compare to the size of the particles so that each particle can be considered as an elastic half-space. We call $R_1^{'}, R_1^{''}$ the principal radii of curvatures of the surface of particle 1 at point O, where $R_1^{'}$ is the maximum value and $R_1^{''}$ is the minimum value of the radius of curvature of all cross-sections of the particle 1's surface at point O. Similarly, we denote $R_2^{'}, R_2^{''}$ the principal radii of curvature of the surface of particle 2 at point O. The angle of orientation between the axes of principal directions of each surface is α. When two particles are pressed against each other by a compressive force F, both the particles locally deform at point O and the contact zone increases. During the compression, the distant points in two particles move towards the point O and parallelly to z axis by displacements δ_1, δ_2 for particle 1 and 2, respectively. Let $\delta = \delta_1 + \delta_2$ denote the total displacement of distant points of two particles under compression. The relation between the force F and the displacement δ is given by [25]

$$F = \frac{4}{3}\frac{\sqrt{R_e}E^*}{F_2^{3/2}}\delta^{3/2} = k_e\delta^{3/2}, \tag{1}$$

where the equivalent radius R_e is defined as

$$R_e = \left(R^{'}R^{''}\right)^{1/2}. \tag{2}$$

R', *R''* are the principal relative radii of curvature and are determined from the principal radii of curvature of two ellipsoidal particles' surfaces at the point O by

$$R^{'} = \frac{1}{(A+B)-(B-A)}, R^{''} = \frac{1}{(A+B)+(B-A)}, \tag{3}$$

where

$$A+B=\frac{1}{2}\left(\frac{1}{R_1^{'}}+\frac{1}{R_1^{''}}+\frac{1}{R_2^{'}}+\frac{1}{R_2^{''}}\right),$$
$$B-A=\frac{1}{2}\left[\left(\frac{1}{R_1^{'}}-\frac{1}{R_1^{''}}\right)^2+\left(\frac{1}{R_2^{'}}-\frac{1}{R_2^{''}}\right)^2+2\left(\frac{1}{R_1^{'}}-\frac{1}{R_1^{''}}\right)\left(\frac{1}{R_2^{'}}-\frac{1}{R_2^{''}}\right)\cos 2\alpha\right]^{1/2}. \quad (4)$$

The contact modulus E^* is given by

$$\frac{1}{E^*}=\frac{1-\nu_1^2}{E_1}+\frac{1-\nu_2^2}{E_2}, \quad (5)$$

where E_1, ν_1, E_2, ν_2 are the elastic moduli and Poisson ratios of the materials for particle 1 and 2, respectively (E_1=E_2 and ν_1=ν_2 in the particular setup studied in this paper). The correction factor F_2 depends on the eccentricity of the elliptical contact area *e* by the following relation

$$F_2=\frac{2}{\pi}K(e)\left\{\frac{4}{\pi e^2}\sqrt{\left[(a/b)^2E(e)-K(e)\right]\left[K(e)-E(e)\right]}\right\}^{-1/3}, \quad (6)$$

where *K(e)*, *E(e)* are the complete elliptic integral of the first and second kind. The eccentricity of the elliptical contact area is given by $e=\left[1-(b/a)^2\right]^{1/2}$, where *b* and *a* are the semi-minor and semi-major axes of the ellipse respectively and the ratio *b/a* can be approximately determined by $b/a\approx\left(R^{'}/R^{''}\right)^{-2/3}$.

It is important to note that the contact law for circular contact area between two spherical particles, $F=k_c\delta^{3/2}$ with the contact stiffness $k_c=\frac{4}{3}\sqrt{\frac{R_1R_2}{R_1+R_2}}E^*$ [25], is just a special case of the elliptical contact law (Eq. (1)). Indeed if we take the limits of $R_1^{'}=R_1^{''}=R_1$ and $R_2^{'}=R_2^{''}=R_2$ the ellipsoidal particles become spherical, the ratio *b/a* becomes 1 which implies that the contact area now is a circle, and the stiffness k_e in Eq. (1) can be shown to degenerate to

k_c in circular contact law. Interestingly, the stiffness k_e in the elliptical contact law is a function of the orientation angle α between the two ellipsoidal particles (see Eq. (4)), differently from the contact law between two spherical particles.

In our experimental setup, two adjacent ellipsoidal particles are assumed to be in point contact at O as shown Fig. 1(b), and the orientation angle α between the particles is considered approximately 0^0. All the ellipsoidal particles in the chain are uniform, therefore, the principal radii of curvature for the surfaces of all the particles have the same values at O and they can be calculated based on the geometry of the particles as $R_1^{'} = R_2^{'} = (L/2)^2 / (D/2) =$ 10.93 mm and $R_1^{''} = R_2^{''} = D/2 = 2.36$ mm.

IV. Solitary Wave Propagation in a Chain of Ellipsoidal Particles

The dynamic response of a "weakly" compressed chain of uniform spherical particles has been captured by a highly nonlinear wave equation, which was derived by Nesterenko employing a long wavelength approximation [1,2]. The solution of this equation showed the existence of compact solitary pulses propagating through the chain with a constant spatial width (~5 times the particle diameter *D*). The solitary wave speed V_s in the chain of spherical particles shows a nonlinear dependence on the normalized force $f_r = F_m / F_o$, where F_m is the maximum dynamic contact force in the chain and F_o is the initial compressive force applied to the chain, which is very small with respect to F_m as [13]

$$V_s = D\sqrt{\frac{4}{5}\frac{k_c^{2/3}}{m}}F_0^{1/6}\frac{1}{f_r^{2/3}-1}\left[\frac{3}{2}+f_r^{5/3}-\frac{5}{2}f_r^{2/3}\right]^{1/2}. \qquad (7)$$

Chains of "weakly" compressed ellipsoidal particles are expected to support an analogous dynamic behavior, since the contact interaction laws for ellipsoidal and spherical particles are

similar, differing only in the expression of the elastic coefficient k_e. The analytical formulations describing wave propagation in a chain of uniform ellipsoidal particles can therefore be obtained following Nesterenko's approach [2]. Accordingly, the nonlinear relation between solitary wave speed V_s and normalized force f_r in a chain of ellipsoidal particles is

$$V_s = D\sqrt{\frac{4}{5}\frac{k_e^{2/3}}{m}}F_0^{1/6}\frac{1}{f_r^{2/3}-1}\left[\frac{3}{2}+f_r^{5/3}-\frac{5}{2}f_r^{2/3}\right]^{1/2} . \quad (8)$$

Here D is the particle size in the direction of the chain (for example, the major or minor axis).

V. Discrete Particle Simulations

We performed discrete particle (DP) simulations to validate the analytical model and for comparison with the experimental results. Following previous investigations [9,13,15,16], we modeled a chain composed of N uniform ellipsoidal particles as a one-dimensional system, where the ellipsoidal particles are treated as point masses connected by nonlinear springs according to the elliptical contact law in Eq. (1). The equation of motion of i-th particle is given by

$$\ddot{u}_i = \frac{\left(k_e\right)_{i-1,i}}{m_i}\left[u_{i-1}-u_i\right]_+^{3/2} - \frac{\left(k_e\right)_{i,i+1}}{m_i}\left[u_{i+1}-u_i\right]_+^{3/2} + g . \quad (9)$$

where u_i is the displacement of the i-th particle ($i \in [1,\ldots, N]$), $(k_e)_{i,j}$ denotes the contact stiffness between i-th particle and j-th particle, m_i is the mass of i-th particle, g is gravitational acceleration, and $[x]_+$ denotes the positive part of x. The particle i=0 represents the striker, and the particle i=N+1 represents the wall (this particle is fixed and its radii of principal curvatures at the point of contact with N-th ellipsoidal particle are infinite). Our discrete particle simulations include the effect of gravitational force to incorporate the vertical arrangement of the experiment

setup. For the sake of simplicity, we have neglected the effect of dissipation in the short chain of ellipsoidal particles that we studied experimentally, as described in Section II. The numerical solutions of Eq. (9) were found by using the fourth order Runge-Kutta method.

VI. Finite Element Simulations

We modeled a chain of 20 uniform ellipsoidal particles, a striker and a rigid plate (the end wall) using a finite element (FE) model generated in Abaqus/CAE. The ellipsoidal particles were modeled as solid (continuum) three-dimensional elements with major and minor axis corresponding to the particles utilized in the experiments. We meshed the volume with tetrahedral elements of second order, using modified 10-node tetrahedral (C3D10M). To get a better representation of the contact interaction, a denser mesh was used in the vicinity of the contact point, as shown in Fig. 2(a). The material parameters of the ellipsoidal particles such as density, Young's modulus, Poisson's ratio of ellipsoidal particles in FE simulation were the same as in the experimental setup. The end wall was modeled as a flat rigid body composed of R3D3 type of elements. The contact interactions between two bodies were defined using the surface-to-surface interaction (Explicit) in Abaqus, where one of the surfaces is selected as master and the other as slave. The constraints applied on the contacts were of small-sliding kinematic with no friction in the tangential direction and contact pressure-over closure in the normal direction. These properties ensured that the two contacting bodies would not penetrate or overlap with each other. More about the Abaqus element and contact details can be found in [26].

To validate the FE model, we computed the static contact interaction between two particles and compared the force-displacement relationship with theoretical results based on Hertzian elliptical contact law (Eq. 1). We perform benchmark tests of the contact force (F) - displacement (δ) relation for three different cases: (i) two ellipsoidal particles contacting at the tip of their minor

axis with the angle of orientation between them is zero (similar to our experimental setup), (ii) two ellipsoidal particles contacting at the tip of their major axis, and (iii) two equivalent spherical particles, i.e. two spheres having the same mass as the ellipsoidal particles, in contact with each other (Fig. 2a). In these simulations the lower particle was held firm by applying fixed boundary conditions and the upper particle was given a displacement boundary condition. The displacement applied to the upper particle was small enough (less than 1% of characteristic dimension in each case, for example the ellipsoidal particle's minor axis in the first case) to ensure the validity of the small displacements assumption in Hertz theory. In the range of forces considered in the experiments described in this paper, the contact force-displacement relations obtained from FE simulations are in good agreement with the theoretical predictions using the Hertzian elliptical contact law (see Fig. 2(b)).

VII. Results and Discussion

We compared force-time responses measured by the instrumented particles in experiments with the corresponding forces obtained from the discrete particle and finite element simulations in Fig. 3(a). Experiments were performed for a chain of 20 ellipsoidal particles arranged along their minor axis. Figure 3(a) presents results obtained when the spherical striker excited the propagation of single pulses with an impact velocity of 0.626 m/s. It is evident that the system supports the formation and propagation of highly nonlinear solitary waves. The width of the solitary wave was measured to be approximately 5.5 particle minor diameters (D). The experimental results are in very good agreement with both the discrete particle and finite element simulation, with the exception for the presence of dissipation in experiments. The solitary wave speed was calculated to be 524 m/s from discrete particle simulation, 529 m/s from FE simulation and 490 m/s from experimental data. The small difference between experimental and

numerical values is probably due to the effect of dissipation, also evident in the amplitude decay noticeable in experiments (compare the pulse amplitude of particle 12 in Fig. 3(a)). The results obtained with the one-dimensional discrete particles model and the three-dimensional FE model are in excellent agreement with each other (see Fig. 3(a)), confirming the validity of the point mass approximation to study one-dimensional ellipsoidal particle dynamics.

We studied the dependence of the solitary wave speed (V_s) on the dynamic force amplitude ($F_{m,e}$) in Fig. 3(b). To compare the experimental results with the theoretical force (F_m)-velocity (V_s) relation obtained from Eq. (8) we calculated numerically the coefficient β as in [9]. The coefficient β is defined as a ratio of the maximum dynamic force on the particle contacts $F_{d,n}$ to the maximum average of the dynamic forces acting on the two contacts of the given particle $F_{m,n}$ as $\beta = F_{d,n}/F_{m,n}$. It should be noted that, both $F_{d,n}$ and $F_{m,n}$ are obtained in discrete particle simulations. The maximum contact force F_m between particles, used in the analytical formulation (Eq. (8)), can be expressed as [9]:

$$F_m = \beta F_{m,e} + F_0 , \qquad (10)$$

where $F_{m,e}$ is the experimentally measured force in the instrumented particles and F_0 is the initial precompression (caused by gravitational loading in our experimental set up) which is selected as a constant value equal to the gravitational compressive force at the midpoint between the two sensors in the chain. We find a very good agreement between the theoretical predictions, experiments and the numerical models (Fig. 3(b)), showing that chains of ellipsoidal particles support robust formation of highly nonlinear solitary waves. This is the first experimental demonstration of highly nonlinear solitary wave propagation in an array of irregular, ellipsoidal particles. It is interesting to note that, despite the inherent non-uniformity of the particles' dimensions, stable solitary waves form and propagate through the chain.

Similar to the response of a chain of spherical particles, the behavior of solitary waves in a chain of ellipsoidal particles can be tuned by varying the radius and/or the elastic modulus of the particles, the initial precompression applied to the system and the amplitude of the dynamic loading [13]. In addition, a chain of ellipsoidal particles, similarly to elliptical disks [23], can be tuned by varying geometric parameters (e.g. the particles relative angular orientation or their stacking directions, such that their major or minor axes are oriented along the direction of wave propagation). We show tunability of the system by analyzing the solitary waves' response with the particles relative orientation using the theoretical and the numerical approaches (Fig. 3(b)). In particular, we study the wave propagation properties when the ellipsoidal particles are aligned along their major axis. For this system's geometry we calculate the stiffness constant k_e in Eq. (1) using Eqs. (2-6). The theoretical value of the stiffness constant k_e for the particles stacked along their minor axis direction is 7.48×10^9 N/m$^{3/2}$, and for particles stacked along their major axis direction is 3.31×10^9 N/m$^{3/2}$. It should be noticed that varying the particle's alignment also varies the particle's size parameter D in Eq. (8), which changes from minor diameter to major diameter. We compared the response of the chains of ellipsoidal particles oriented along the particles' major and minor axis to the response of a chain of equivalent spherical particles. Equivalent spherical particle are defined as particles having the same mass of the ellipsoidal particle and the radius $r = \left(\frac{3}{4\pi} m \right)^{1/3}$. The relationship between solitary wave velocity (V_s) and dynamic loading (F_m) for a chain of spherical particles can be obtained theoretically using Eq. (7) [13]. We compared results from the discrete particle model, finite element analysis and theory for two chains of ellipsoidal particles with different arrangements (chain with all the ellipsoidal particles arranged in minor and major axis direction, respectively) and for the chain of spherical particles, and we find excellent agreement. From Fig. 3(b) it is evident that, when the particles in the

system are oriented along their minor axis along the chain, the velocity of the solitary wave is slower than the velocity of solitary wave in a chain of equivalent spherical particles excited with the same dynamic loading (this is due to the fact that in this case the ellipse minor axis is smaller than the diameter of equivalent sphere). Following similar geometric considerations, when the particles in the system are oriented along their major axis, the velocity of the solitary wave is faster than the velocity of solitary wave in a chain of equivalent spherical particles excited with the same dynamic loading.

We studied the effects of dissipation testing a longer chain composed of 50 elliptical particles, excited by a steel striker (m_s = 0.45 g) with different impact velocities (0.37 m/s, 0.49 m/s and 0.66 m/s). We inserted 4 sensors in particle number 8, 16, 28 and 41 from the top, and monitored the amplitude decay and the variation of the pulse shape as the wave propagated through the system (Fig. 4). We compared the results with a modified discrete particle model that includes linear damping term following the model described in [27] as

$$\ddot{u}_i = \left\{ \frac{(k_e)_{i-1,i}}{m_i} \left[u_{i-1} - u_i\right]_+^{3/2} - \frac{(k_e)_{i,i+1}}{m_i} \left[u_{i+1} - u_i\right]_+^{3/2} \right\} + \gamma s \left| \left[\dot{u}_{i-1} - \dot{u}_i\right]_+ - \left[\dot{u}_{i+1} - \dot{u}_i\right]_+ \right| + g \,. \qquad (11)$$

where γ is the relaxation (dissipation) coefficient, s is the sign of $\left(\left[\dot{u}_{i-1} - \dot{u}_i\right]_+ - \left[\dot{u}_{i+1} - \dot{u}_i\right]_+ \right)$.

Results show that a chain of 50 particles presents significant dissipation. The linear damping model captures well the wave amplitude decay and the changes of wave shape in the whole range of impact velocities studied (Fig. 4). The relaxation coefficient γ in each experiment was determined by minimizing the root mean square (RMS) difference between the experimental force amplitude $F_{m,e}$ at each sensor location and the corresponding numerical one. The optimal value of relaxation coefficient γ was found to vary from -15.55 to -3.18 in the range of impact velocities tested in experiments.

The system described in this paper can be used to create two- and three-dimensional crystal structures of ellipsoidal particles in cubic packing arrangement. These high dimensional media provide the directional dependence for stress wave propagation. The difference in stress wave propagation speeds in selected directions can be controlled by choosing appropriate values of major and minor axis of ellipsoidal particles in the structures.

VIII. Conclusions

The impulse propagation in a one-dimensional chain of uniform ellipsoidal particles was studied using theoretical analysis, experiments and two separate numerical approaches (one-dimensional discrete particle model and finite element analysis).We reviewed the fundamental principles of the contact interaction between two ellipsoidal particles, and utilized the contact law to study analytically the dynamics of a chain of ellipsoidal particles. We observed the formation and propagation of highly nonlinear solitary waves finding good agreement between experiments, theory and the numerical analyses. We show the effects of particle orientation on the pulse propagation velocity in the chains, and we study the effects of dissipation in a longer chain of particles. These observations demonstrate that the particles' geometry and relative orientation offer additional mechanisms to tune the stress propagation in granular chains, of interest for the design of new materials capable of tailoring stress propagation and for the development of tunable acoustic devices.

IX. Acknowledgements

We thank Mr. Richard E. Baumer for help in experiments. C.D. acknowledges support from the Army Research Office (Proposal No. 54272-EG, and ARO/MURI) and the National Science Foundation (NSF/CMMI-844540-CAREER).

Figure Captions

Figure 1. (Color online) (a) Digital image showing the ellipsoidal particles used in experiments. (b) Schematic diagram showing the front and side view for the contact between two ellipsoidal particles and the dimensions and the radii of the maximum and minimum principal of curvatures at the contact points between ellipsoidal particles. (c) Schematic diagram for assembly of a 20 particles chain of vertically stacked stainless steel ellipsoidal particles. Piezoelectric sensors were embedded in particles 7, 12. (d) Schematic diagram representing the assembly of the piezogauges embedded inside selected ellipsoidal particles.

Figure 2. (Color online) (a) Finite element mesh of: (i) two adjacent ellipsoidal particles arranged in the minor axis direction; (ii) two adjacent ellipsoidal particles arranged in the major axis direction; (iii) two adjacent equivalent spherical particles. (b) Comparison of the contact force-displacement relations between two ellipsoidal particles arranged in minor (curve group (i)) and major (curve group(ii)) axis direction, and also between two equivalent spherical particles (curve group(iii)) obtained from both finite element simulations (dotted (blue) curves) and Hertzian elliptical contact law (solid (black) curves).

Figure 3. (Color online) (a) Comparison of experiments and numerical results on the formation and propagation of a solitary wave in a chain of 20 stainless steel ellipsoidal particles excited by impacting a stainless steel spherical striker of mass m=0.925 g with an initial velocity of 0.626 m/s. Curve group1 shows the results for particle 7 in the chain from the top, and similarly, curve group2 shows the results for particle 12 from top. Experimental results are shown by solid (green) curves. (b) Dependence of the wave speed on the maximum contact dynamic force in the

chains of ellipsoidal particles arranged in both minor (curve group (i)) and major (curve group (ii)) axis directions and in the chain of equivalent spherical particles (curve group (iii)) under gravitational loading. Experimental data for chain of ellipsoidal particles arranged in minor axis direction are shown by solid (green) diamonds in curve group (iii). The solid (black) curves represent the theoretical predictions. In both panels the dashed (red) curves represent the discrete particle results, the dotted (blue) curves represents the finite element results.

Figure 4. (Color online) Experimental results obtained in a chain composed of 50 particles, excited by a striker with an impact velocity v =0.37 m/s. The (green) solid curves represent force-time signals obtained from instrumented particles positioned in location 8, 16, 28 and 41. The (red) dashed curves represent numerical results obtained from a modified discrete particle model (DPM) with linear damping. γ is the relaxation coefficient and has a value of -11.67.

Figure 1

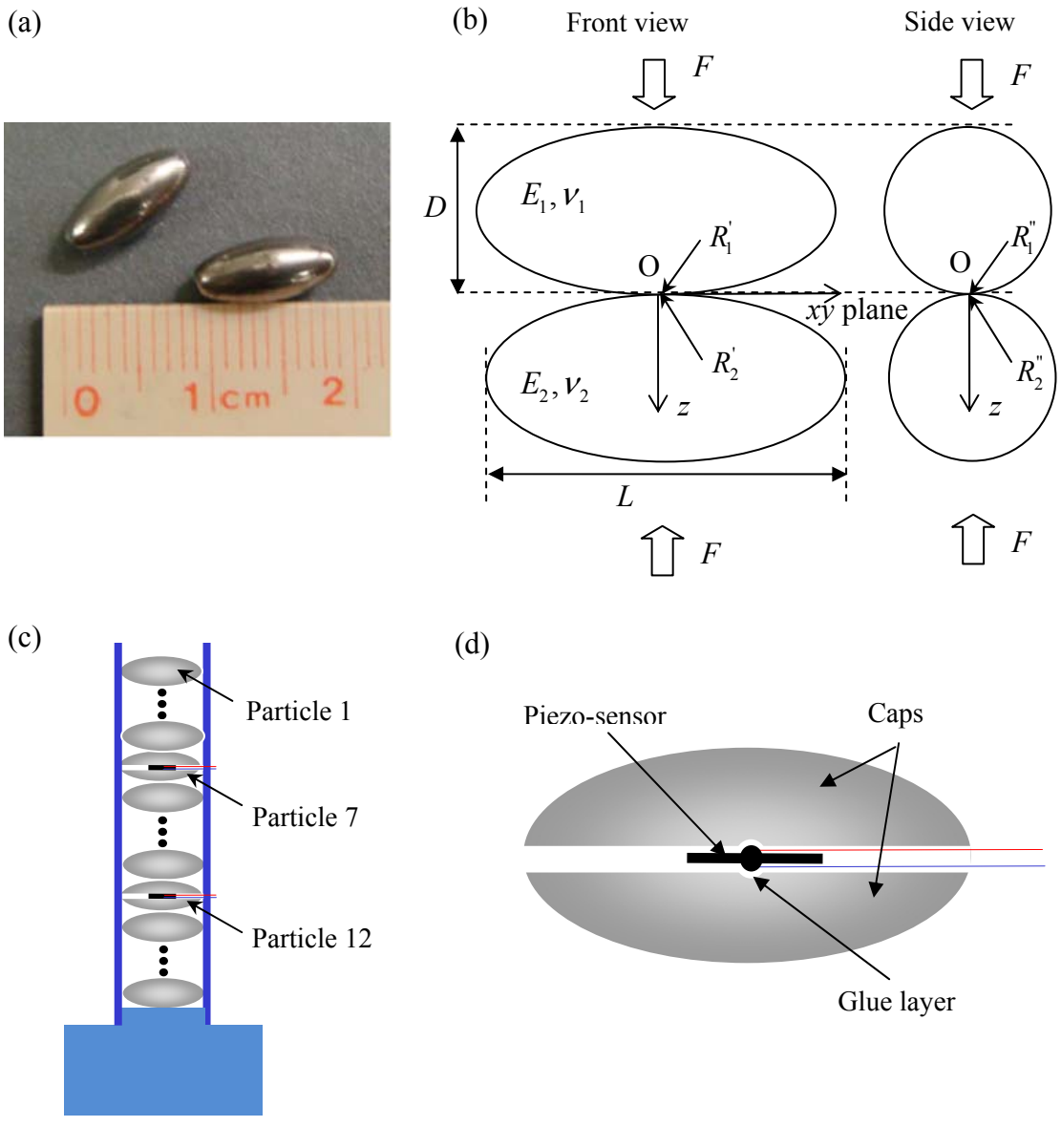
(a)
0
1 cm
2
(b)
Front view
Side view
F
F
D
E_1, ν_1
R_1'
O
O
R_1''
xy plane
E_2, ν_2
R_2'
R_2''
z
z
L
F
F
(c)
Particle 1
Particle 7
Particle 12
(d)
Piezo-sensor
Caps
Glue layer

Figure 2

(a)

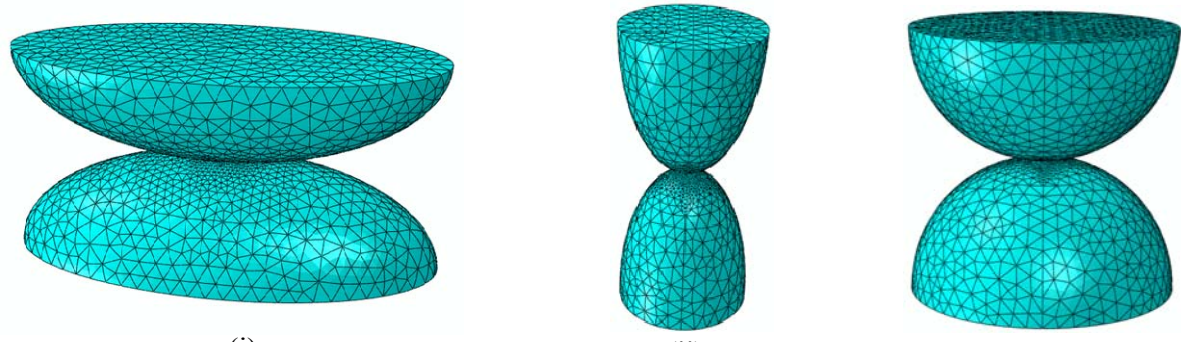

(i) (ii) (iii)

(b)

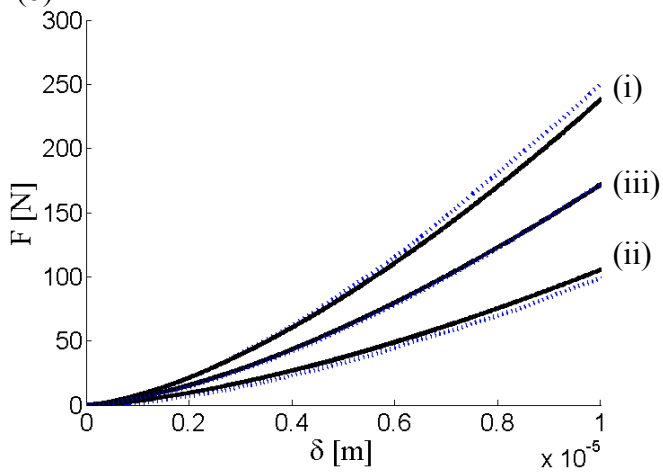

Figure 3

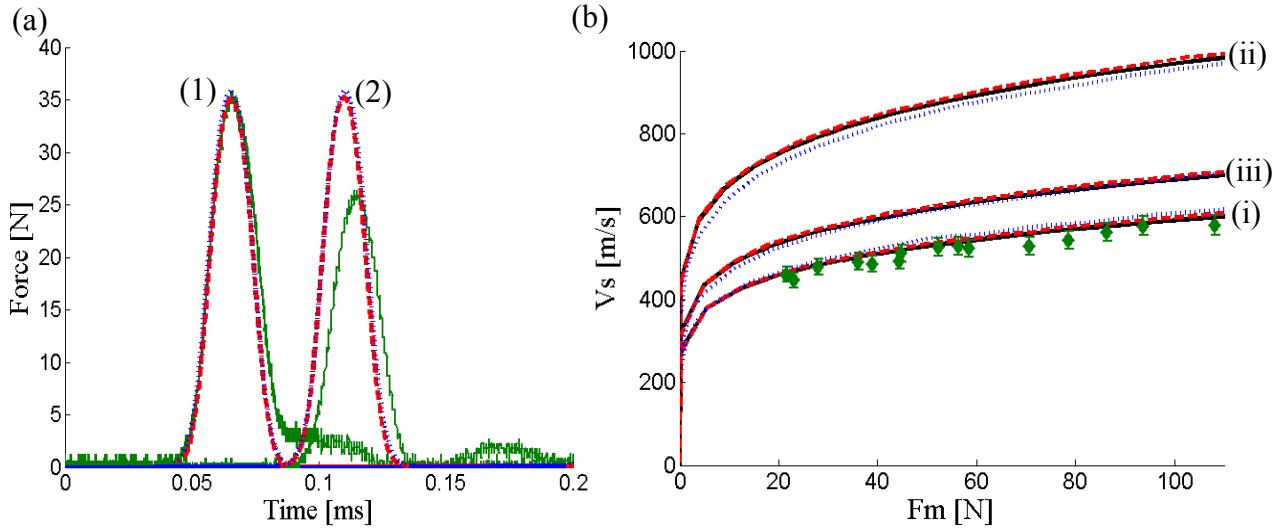

Figure 4

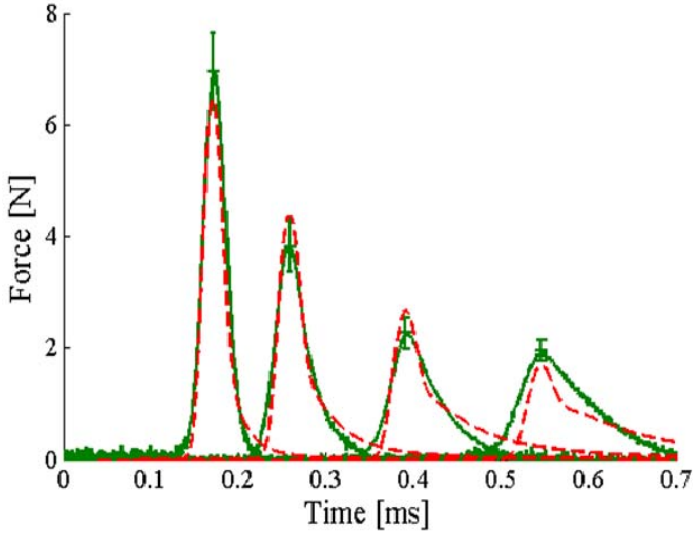

References

1. V.F. Nesterenko, Prikl. Mekh. Tekh. Fiz. **24**, 136 (1983); J. Appl. Mech. Tech. Phys. **24**, 733 (1984).
2. V.F. Nesterenko, *Dynamics of Heterogeneous Materials* (Springer-Verlag, New York, 2001)
3. S. Sen, J. Hong, J. Bang, E. Avalosa, and R. Doney, Phys. Rep.**462**, 21 (2008).
4. A. N. Lazaridi and V.F. Nesterenko, Prikl. Mekh. Tekh. Fiz. **26**, 115 (1985); J. Appl. Mech. Tech. Phys. **26**, 405 (1985).
5. C. Coste, E. Falcon, and S. Fauve, Phys. Rev. E**56**, 6104 (1997).
6. A. Chatterjee, Phys. Rev. E **59**, 5912 (1999).
7. J. Hong, Phys. Rev. Lett. **94**, 108001 (2005).
8. S. Job, F. Melo, A. Sokolow, and S. Sen, Phys. Rev. Lett. **94**, 178002 (2005).
9. C. Daraio, V.F. Nesterenko, E.B. Herbold, and S. Jin, Phys. Rev. E**72**, 016603 (2005).
10. V.F. Nesterenko, C. Daraio, E.B. Herbold, and S. Jin, Phys. Rev. Lett. **95**, 158702 (2005).
11. L. Vergara, Phys. Rev.E**73**, 066623 (2006).
12. R. Doney, S. Sen, Phys. Rev. Lett. **97**, 155502(2006).
13. C. Daraio, V.F. Nesterenko, E.B. Herbold, and S. Jin, Phys. Rev. E**73**, 026610 (2006).
14. S. Job, F. Melo, A. Solokow, and S. Sen, Granular Matter**10**, 13 (2007).
15. M.A. Porter, C. Daraio, E.B. Herbold, I. Szelengowicz, and P.G. Kevrekidis, Phys. Rev. E**77**, 015601 (2008).
16. M.A. Porter, C. Daraio, E.B. Herbold, I. Szelengowicz, and P.G. Kevrekidis, Physica D**238**, 666(2009).
17. U. Harbola, A. Rosas, A.H. Romero, M. Esposito, and K. Lindenberg, Phys. Rev. E **80**, 051302 (2009).
18. A. Molinari and C. Daraio, Phys. Rev. E **80**, 056602 (2009).
19. C. Daraio, V.F. Nesterenko, E.B. Herbold, and S. Jin, Phys. Rev.Lett. **96**, 058002 (2006).
20. E.B. Herbold, J. Kim, V.F. Nesterenko, S. Wang, and C. Daraio, Acta Mech. **205**, 85 (2009).
21. F. Fraternali, M.A. Porter, and C. Daraio, Mech. Adv. Mat. Struct. **17**, 1(2010).
22. A. Spadoni, and C. Daraio, Proc. Natl. Acad. Sci. USA**107**, 7230 (2010).
23. A. Shukla, M.H. Sadd, R. Singh, Q. Tai and S. Vishwanathan, Optics and Lasers in Engineering **19**, 99-119 (1993).
24. http://www.efunda.com, http://mat.web.com.
25. K. L. Johnson, *Contact Mechanics*(Cambridge University Press,1985).
26. Simulia, Abaqus version 6.8 Documentation, D.S.S.A., Editor. (Providence, RI,2008).
27. R. Carretero-Gonzalez, D. Khatri, M.A. Porter, P.G. Kevrekidis, and C. Daraio, Phys. Rev. Lett. **102**, 024102 (2009).